

Interferometric Studies of Faster than Sound Phenomena. Part I. The Gas Flow around Various Objects in a Free, Homogeneous, Supersonic Air Stream

R. LADENBURG, J. WINCKLER, AND C. C. VAN VOORHIS

Palmer Physical Laboratory, Princeton University, Princeton, New Jersey

(Received December 1, 1947)

A small Mach-Zehnder interferometer is used for analysis of the supersonic air flow in a free homogeneous jet of cylindrical symmetry ("open wind tunnel") at Mach number 1.70 and around various simple objects suspended in it. The interferograms obtained can be evaluated because of the axial symmetry of the phenomena, and this process is carried out by integration of the Abel equation. This "open wind tunnel" does not need any windows; however, the working section is rather restricted, especially by the intersection of the head wave of a suspended body under investigation with the free boundary of the jet. Also the turbulent free jet boundary itself is a source of disturbance. The density, pressure, temperature, velocity, and Mach number throughout the air flow have been determined with reasonable accuracy. For suspended cones of 10° and 30° semi-angle the theory of Taylor-Maccoll has been verified—except near the cone tip where a systematic

density increase occurred. For a 45° semi-angle cone and a small sphere where a detached curved shock wave appears, no theoretical results exist at present. However, stream and Mach lines were constructed with the help of the measured density distribution and of the conventional equations for compressible fluids, and pressure coefficients on the surface of the objects were calculated. The results show that the rotational effects are small at the present Mach number. The experience obtained with the small interferometer indicates that it is a very valuable instrument in studying supersonic phenomena, and that it will yield accurate quantitative results not obtainable by other methods. Undoubtedly, it can be applied to a modern supersonic wind tunnel, and such investigations are being undertaken with a larger interferometer and associated equipment.

I. INTRODUCTION

OPTICAL methods for the study of phenomena in fluid mechanics are superior to all other methods as they do not disturb the gas flow in any way. Three such optical methods are known: (1) the shadowgraphic method, which reacts essentially upon the second derivative of the density and is therefore extremely sensitive to sudden changes of density, especially to shocks as they appear in supersonic (that is, "faster than sound") phenomena; (2) the striae or schlieren method, which depends upon the first derivative of the density and reacts, therefore, even to slow changes; (3) and the interferometric method, which gives directly the density itself, and that quantitatively. Once the density of a gas stream is known, it is often possible to compute also its pressure, temperature, and velocity on the basis of well-known hydrodynamic relations for compressible gases.

The most suitable instrument for interferometric work is the Mach¹-Zehnder² interferom-

eter, a modification of the Jamin instrument. It divides the incoming light into two coherent beams widely separated so that phenomena in one of these beams do not disturb the other beam (see Fig. 1). A further advantage of this instrument is that by suitable adjustments of the plates the interference fringes can be produced in any plane, so that the fringes may be focused simultaneously with the gas stream upon a photographic plate and so record the density changes produced by the moving gas. Such an instrument has been used by E. and L. Mach¹ and by C. Cranz and his collaborators and pupils for the study of the supersonic gas flow in jets and for the disturbances produced by projectiles fired with supersonic velocity. We have carried out such interferometric investigations of various supersonic phenomena. The present paper, the first of a series, contains the results obtained on the gas flow around various objects suspended in a free, homogeneous, supersonic air stream,

¹ E. Mach and L. Mach, *Wien. Akad. Ber. math.-phys. Klasse* **98**, 1318 (1889); L. Mach, *Zeits. f. Instrumentenk.* **12**, 89 (1892); *ibid.* **14**, 279 (1894); see C. Cranz, *Lehrbuch*

der Ballistik (1926), volume II, §23; *ibid.* (1927), volume III, §80-82; *ibid.* (1936), *Ergaenzungsband*, §69.

² L. Zehnder, *Zeits. f. Instrumentenk.* **11**, 275 (1891).

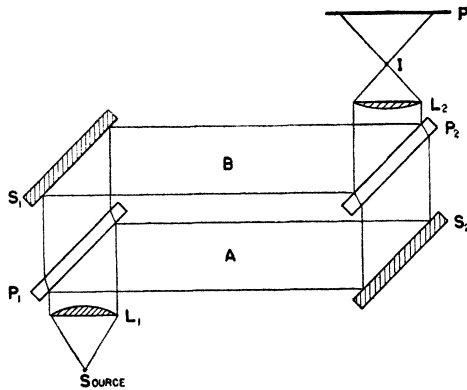


FIG. 1. Mach interferometer.

that is, in a kind of open, intermittent wind tunnel.³

The theory of the Mach-Zehnder interferometer has been given by various authors.⁴ Details of the instrument used in the present paper, its adjustment and some of its applications are described by one of the present authors (J. W.) in another journal.⁵

II. EXPERIMENTAL METHOD

A. Instrumentation

The interferometer used (Fig. 1) rests on angle irons which, in turn, are supported by concrete pillars and insulated by rubber cushions against vibration. The object of the present investigations is a supersonic air jet, usually located in the light beam *B* of Fig. 1 between the mirror *S*₁ and the beam splitting plate, *P*₂. It produces the displacements of the interference fringes which are straight and equidistant without the jet. The interferometer plates of 6×3 cm size are the property of Dr. R. B. Kennard who was kind enough to lend them for the present experiments, and who, following our request, also directed the construction of the plate holders at the shop of the National Bureau of Standards. Dr. Kennard had used these plates some years ago for the

study of temperature distribution and heat flux in air by interferometry.⁶ The plates can be rotated by screws around a horizontal and a vertical axis and so adjusted that they give sharp interference fringes of a monochromatic light source, in any direction and in any plane desired. For details of the technique of adjusting the instrument see reference 5.

The air jet for investigation was supplied from a 1½-m³ tank which was filled with dry air at pressures up to 120 lb./in.² fed from high pressure gas cylinders pumped up on a liquid-air machine. The pressure *p*₀ and temperature *t*₀ of the air in the tank could be measured accurately. The compressed air escaped from the tank through a streamlined neck, and then passed through a valve which formed a smooth passage when open into a kind of Laval nozzle (see Fig. 2) and emerged as a parallel, homogeneous, supersonic stream at atmospheric pressure. The valve could be opened and closed by hand within one or two seconds. The expanding portion of the nozzle was shaped according to designs of Mr. Alan Puckett of the Guggenheim Aeronautical Laboratory, California Institute of Technology, to give a Mach number of about 1.7. The "throat" is actually the straight portion between *D* and *C* of Fig. 2. The ratio between the throat area, *A*, and the final section area, *A*₁, determined the final Mach number, *M*, according to the relation

$$\frac{A}{A_1} = \frac{1}{M} \left(1 + \frac{\gamma - 1}{2} M^2 \right)^{\frac{1}{2}(\gamma + 1)/(\gamma - 1)} \quad (1)$$

where

$$\gamma = C_p/C_v = 1.404 \text{ (for air).}$$

The numerical table in Fig. 2 gives the data from which the nozzle was shaped. No consideration was given to the effect of the boundary layer on effective nozzle diameter, nevertheless the Mach number actually was found to be very close to 1.70. The long throat, in which the Mach number is theoretically unity, is probably an undesirable feature as the gas flows at high speed near the wall for a finite time. The turbulence arising from this, as well as that from the boundary of the free jet in the atmosphere, is

³ The work described here was started in 1944 under the sponsorship of the Office of Scientific Research and Development, and was taken over in 1945 by the Bureau of Ordnance of the Navy Department under Contract NORD 9240. Short abstracts appeared in *Phys. Rev.* **69**, 251 (1946) and **71**, 464 (1947).

⁴ C. Cranz, reference 1; G. Hansen, *Zeits. f. tech. Physik* **12**, 436 (1931); H. Schardin, *Zeits. f. Instrumentenk.* **53**, 396, 424 (1933); W. Kinder, *Optik* **1**, 413 (1946). These papers also contain references to the complete literature.

⁵ J. Winckler, *Rev. Sci. Inst.* **19**, 307 (1948).

⁶ R. B. Kennard, *J. Research Nat. Bur. Stand.* **8**, 787 (1932).

the main limitation on the over-all accuracy of the present results.

The models were supported in a simple way on the end of an axial rod, which was secured to a cross-piece some distance downstream from the working section. The area viewed by the interferometer extends about 25 mm out from the orifice, and is about 40 mm in width, or slightly greater than the width of the air stream. The actual working section is less than this for reasons which will be discussed later (see Section III, A).

In operation, the tank was filled with dry, compressed air to a pressure slightly higher than the working pressure. The valve lever was turned quickly by hand, and when enough air had escaped to drop the pressure to the working value, an automatic switch discharged the spark which made the photograph. The working tank pressure P_0 , which is necessary to produce the free jet at atmospheric pressure P , is determined by the Mach number according to the relation

$$P_0/P = [1 + \frac{1}{2}(\gamma - 1)M^2]^{\gamma/\gamma - 1}. \quad (2)$$

This pressure was first calculated and finally established by trial (see Section III, A).

The light source used was a magnesium spark excited by a 0.5- μ f capacitor charged to 9000 volts, in connection with a monochromator for isolating the strong violet line 4481A. This line has an intensity about twice that of the underlying continuum and is monochromatic enough to produce about 200 usable fringes, with illumination times of about 1 microsecond and a photographic image of about $1\frac{1}{2} \times 2$ inches. Eastman spectrographic plates, 4 in. \times 5 in., type 103-0, were used for the interferograms. For taking these pictures a special plate holder was equipped with interchangeable slides, running in grooves as close as possible to the front of the plate. One slide consisted of horizontal slits of $\frac{1}{2}$ -mm opening extending across the plate at intervals of 5 mm; the other slide contained $\frac{1}{2}$ -mm diameter wires stretched at the exact position necessary to blank out the slits. Thus it was possible, by use of the slits, to photograph the undisplaced fringes, and then to substitute the wires and repeat the exposure with the jet turned on. Since the fringes are customarily oriented vertically, that is, parallel to the stream-

ing gas, this results in a composite photograph in which the undisplaced fringes are available for reference, so that a correction may be made for optical errors in the system, such as lack of plane-parallelism in the plates, etc. Figure 14 shows a composite interferogram using grids. The undisplaced fringes appear in the narrow bands.

Shadowgrams are made in the parallel light from a point source spark of the type designed by Dr. Charters of the Ballistic Research Laboratory, Aberdeen Proving Ground, and a 70-mm focal length telescope objective. Ordinarily the photographic plate was fixed 25 mm from the jet axis. Schlieren photographs were made in an elementary way with a single lens which focused this same spark on a knife edge, and at the same time focused the jet on the photographic plate placed after the knife edge.

B. Measurement of the Interference Patterns

The purpose of the study is to obtain first of all the fringe shifts in various horizontal cross sections through the vertical flow of the gas stream. If one adjusts the interference fringes in a horizontal direction, that is, perpendicular to the gas flow, one obtains pictures like that in Fig. 12 where a conical object of 30° semi-angle

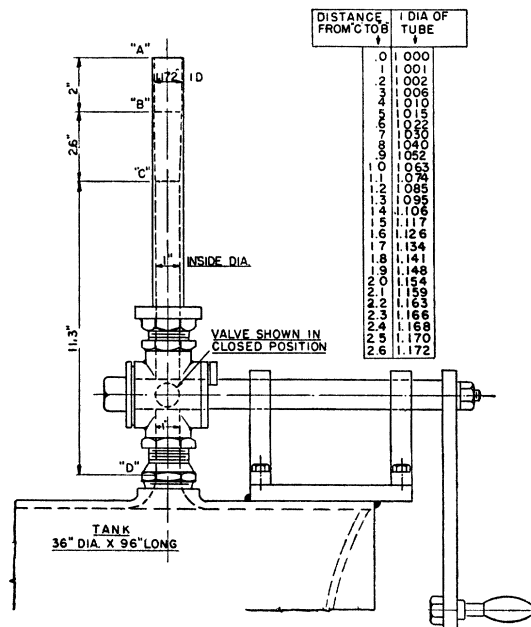


FIG. 2. Orifice and valve assembly.

is supported in the jet. The picture is symmetrical with respect to the vertical axis of the jet as one should expect. In order to get the fringe shifts along a horizontal cross section one has to measure at first the position of each fringe along a series of directions normal to the horizontal fringes and then to transform the shifts of each fringe from its undisplaced position to the various horizontal cross sections. The procedure is simplified if the undisplaced fringes are oriented vertical, that is, parallel to the gas flow (Fig. 14). Now they appear asymmetric with respect to the vertical axis of the jet since they are all shifted to the right or to the left along a horizontal cross section. Therefore they are crowded on one side and widened on the other side. However, if one now measures the shifts of the fringes from their undisplaced positions along a horizontal axis, one obtains without further transformation the desired fringe shifts which are symmetrical with respect to the axis of the jet.

The positions of the undisplaced fringes are obtained on the same photographic plate as the interferograms under measurement, with the help of the horizontal slits and wires described in the previous section. Pictures of the fringes without the jet flowing showed that, due to small inhomogeneities of the interferometer plates, the undisplaced fringes were not quite parallel, uniformly spaced lines, but deviated in

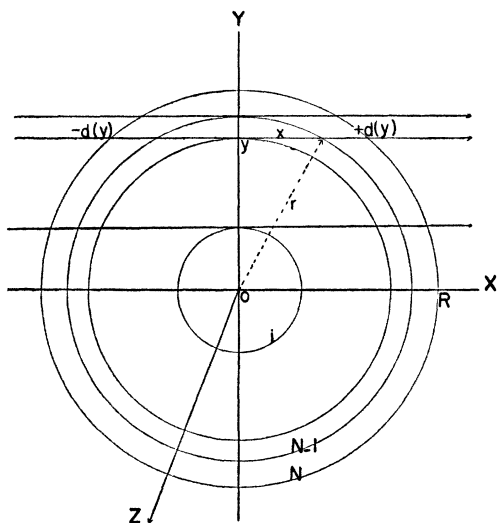


FIG. 3. Horizontal cross section through jet divided into concentric zones of equal width.

some places by as much as 0.4 fringe units from this condition. The correction values were plotted on a map of the area of observation, and this map could then be used to correct, point by point, the fringe shift curves.

The fringe shift values obtained for each cross section were evaluated and plotted completely across the section on transparent paper, producing a nearly symmetrical curve of points. The curve was folded at its axis of symmetry by trial, by use of an illuminated viewing box, and a new curve, representing the average of the two sides, was traced in.

C. Determination of the Density Distribution and its Accuracy

The fringe shifts produced by the streaming gas are due to the differences between its refractive index and that of the air in the other beam of the interferometer. The computation of the density distribution in the streaming gas from the obtained fringe shifts is very simple only in a two-dimensional channel pattern when the density is constant along the light path through the field of view.

Let t be the uniform thickness of the channel along the light path, n_0 and ρ_0 refractive index and density, respectively, of the undisturbed gas in the corresponding light beam of the other arm of the interferometer, and λ the wave-length of the light used. Then the refractive index, n , and density, ρ , at a place where the fringe shift is δ , are given by the simple relations

$$\delta \cdot \lambda = (n - n_0)t = K(\rho - \rho_0)t, \quad (3)$$

where

$$K = (n - 1)/\rho,$$

the Gladstone-Dale constant, depends only on the wave-length and the kind of gas used; therefore,

$$\rho = \rho_0 + (\delta \cdot \lambda)/(K \cdot t).$$

In the present case, the density of the streaming gas is not constant along the light path since the gas escapes through a circular orifice and expands radially as well as in the direction of the jet. Also, various parts of the light beam penetrate different thicknesses of the jet. However, the phenomenon has axial symmetry and can be completely evaluated. Let us assume parallel light and consider a horizontal cross

section through the jet (Fig. 3). Let x again be the direction of the light path, y the other coordinate in this plane, measuring the distance from the axis of the jet, and z the direction of the escaping gas in the jet. Then the fringe shift

$$\delta(y) \cdot \lambda = 2 \int_0^{d(y)} [n(y) - n_0] dx$$

$$= 2 \int_0^R [n(r) - n_0] [r dr / (r^2 - y^2)^{1/2}], \quad (4)$$

where $d(y)$ is half the thickness of the jet at a distance y from the axis, $r^2 = x^2 + y^2$, and R is the radius of the jet in the considered cross section.

A solution of this problem in rough approximation has been given by L. Mach⁷ and by H. Schardin.⁴ They obtain the values of the refractive index of the jet, $n(r)$, by subdividing the cross section considered into many annular zones of radii r where

$$0 = r_0 < r_1 < \dots < r_i < r_{i+1} < \dots < r_N = R,$$

and assuming that $n(r)$ is constant in each zone (Fig. 3). Hence, the value of $n(r_{N-1})$ for the outermost zone between the circles r_N and r_{N-1} is obtained from the fringe shift δ_{N-1} of the beam penetrating this zone in the same way as $n(y)$ is obtained from $\delta(y)$, according to Eq. (3). The next chord traverses only one more zone besides the zone of refractive index $n(r_{N-1})$ —that of refractive index $n(r_{N-2})$ which can be obtained in a similar way. Therefore, Eq. (4) reduces to a simple system of linear equations for the unknown values of the refractive index. Let

$$n(r_i) - n_0 = \begin{cases} \nu_i & \text{for } r_i \leq r \leq r_{i+1}, \\ 0 & \text{for } r \geq R, \end{cases}$$

then

$$\lambda \cdot \delta(y)_{y=r_i} = \lambda \cdot \delta_i = \sum_{\kappa=i}^{N-1} 2\nu_{\kappa} \int_{r_{\kappa}}^{r_{\kappa+1}} \frac{r dr}{(r^2 - r_i^2)^{1/2}}$$

$$= 2 \sum_{\kappa=i}^{N-1} \nu_{\kappa} \{ (r_{\kappa+1}^2 - r_i^2)^{1/2} - (r_{\kappa}^2 - r_i^2)^{1/2} \}$$

$$= 2l \sum_{\kappa=i}^{N-1} \nu_{\kappa} \{ [(\kappa+1)^2 - i^2]^{1/2} - (\kappa^2 - i^2)^{1/2} \}$$

$$= 2l \sum_{\kappa=i}^{N-1} \nu_{\kappa} \cdot a(\kappa, i), \quad (5)$$

⁷L. Mach, Wien. Akad. Ber. math.-phys. Klasse 105, 605 (1896).

when $0 \leq i \leq \kappa \leq N-1$ and if all zones have equal width l so that $r_i = i \cdot l$. A systematic manner of solving this system, provided a master table of the coefficient $a(\kappa, i)$ is available, will be found in the paper by F. J. Weyl "Computational aspects of gas flow interferometry" to appear in this journal. That paper contains also details of a refinement of this procedure suggested by one of the present authors (C.C.V.V.); instead of assuming $n(r)$ constant in each zone one approximates it by a linear function of r :

$$n(r) - n_0 = \nu_i + [(r - r_i) / (r_{i+1} - r_i)] (\nu_{i+1} - \nu_i)$$

for $r_i \leq r \leq r_{i+1}$,

where, as before,

$$\nu_i = n(r_i) - n_0.$$

This approximation leads again to a number of linear equations

$$\lambda \cdot \delta_i = l \nu_i A(i, i)$$

$$+ l \sum_{\kappa=i+1}^{N-1} \nu_{\kappa} \{ A(\kappa, i) - A(\kappa - 1, i) \}, \quad (6)$$

where

$$A(\kappa, i) = (\kappa+1) [(\kappa+1)^2 - i^2]^{1/2} - \kappa (\kappa^2 - i^2)^{1/2}$$

$$- i^2 \log \frac{\kappa+1 + [(\kappa+1)^2 - i^2]^{1/2}}{\kappa + (\kappa^2 - i^2)^{1/2}}, \quad (6a)$$

and the zones are supposed to be of equal width as before.

A large master table of these coefficients for 50 zones is contained in NAVORD Report 69-46.⁸ The use of a larger number of zones in the reduction of a given fringe shift curve, quite apart from the fact that it increases greatly the amount of computational labor involved, does not necessarily entail greater accuracy in the result. It is, therefore, a distinct advantage of this procedure that any particular zone where interesting details exist in the $\delta(y)$ curve can be subdivided. The coefficients to be used for subdivided zones and the procedure for carrying out such computations will be given in Weyl's paper. (More details are contained in NAVORD report 69-46.) Such increase of the resolution is speci-

⁸A photostatic copy of this table may be obtained on request from Palmer Physical Laboratory. In this table the letter κ is replaced by the letter μ . Copies of the NAVORD reports may be obtained from the Bureau of Ordnance, Navy Department, Washington, D. C.

ally useful at shock fronts. The actual shock front, however, is beyond the resolution of optical methods (a few mean free-paths in thickness).

Dr. Hans Panofsky has suggested another procedure for computing the rapid change of refraction index and density at a shock. It consists in inserting a "Schardin zone" just at the shock position by using suitable coefficients. This eliminates "over-shooting" of the computed values, which is apt to occur whenever the actual rate of change of ν in a zone is greater than the assumed linear rate between zone boundaries, and it produces a smooth behavior of the density curve after a shock. Such a "Schardin zone," being a density plateau with a flat top and square front, approximates closely the density behind an actual shock front. Details will be discussed in the paper by F. J. Weyl mentioned above.

The evaluation of the interferograms of jets is partly done by this approximation of Van Voorhis and Weyl, and partly by a still more exact solution of Eq. (4) suggested by J. Von Neumann. Introduction of the variables

$$v = r^2, \quad u = y^2$$

reduces Eq. (4) to

$$\lambda \cdot \delta(u) = \int_u^\infty \frac{\nu(v)}{(v-u)^{\frac{1}{2}}} dv,$$

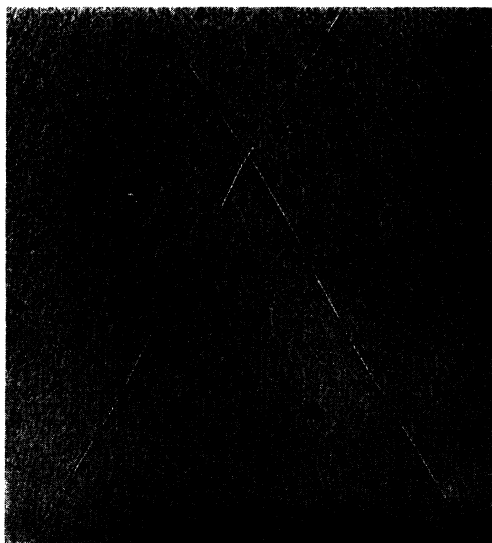


FIG. 4. Shadowgram of the homogeneous jet. $M=1.70$.

where $\nu = n - n_0$ is now a function of v only. Solution of this integral equation is accomplished by applying once more the Abel operator

$$\int_u^\infty [f(v)dv/(v-u)^{\frac{1}{2}}]$$

to both sides of the integral equation. The procedure of this solution has been worked out by F. J. Weyl and will be described in this journal. Also given there is the complete mechanization of the computation with the help of IBM machines, as worked out by H. Polachek, and a discussion of the accuracy obtainable. Coefficients for 100 zones have been worked out for use in this method.

A comparison of the results gained by this method and by the Van Voorhis-Weyl approximation for the same interferogram showed good agreement within the accuracy obtainable, but the use of the IBM machines saves a large amount of labor. It is hoped that the new electronic machines for computation will reduce appreciably the time needed for computation.

From the ν -value one obtains the corresponding values of the density in the jet

$$\rho = \rho_0 + (\nu/K),$$

where K is the Gladstone-Dale constant for the jet of dry air, $K = (n-1)/\rho$, and ρ_0 is the equivalent density of the displaced air, assumed to be half-saturated with water vapor. The zone width l is optional. This calculation is easily carried out on a hand computing machine. For the magnesium line used in the present experiments, $\lambda = 4481\text{\AA}$, one obtains, from the best known values of density and refractive index for air,

$$K = 0.22823 \text{ cm}^3/\text{g}.$$

The absolute values of the densities obtained in the present paper lie between 1 and 5 mg/cm³. An estimate of its accuracy is complicated by the stepwise, accumulative method of evaluating the refractive index. The plotted values of the fringe shifts $\delta(y)$ probably represent accurately the optical effect of the jet within about 0.03 of a fringe shift unit at places of small slope, and within 0.07 at places of large slope. In the extreme case of large slope, if the error occurs at the center, and with a zone width of 0.02 cm, the

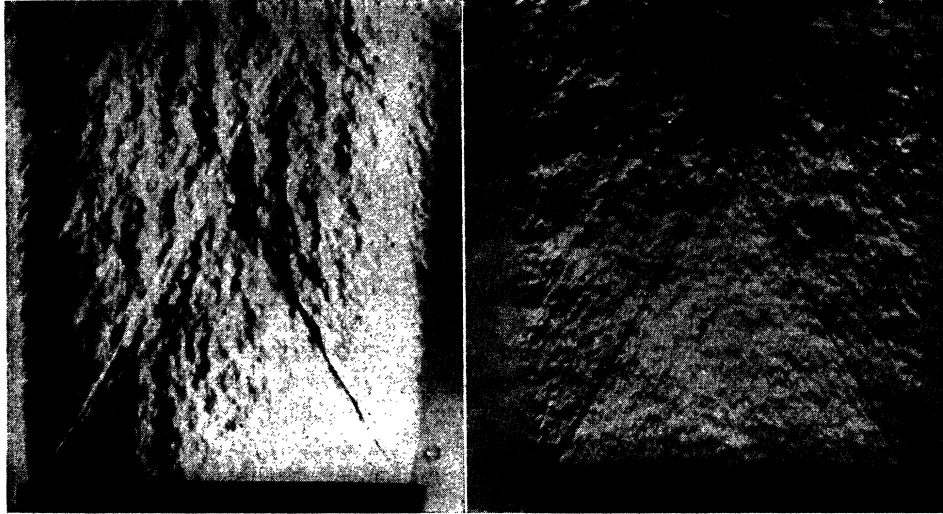


FIG. 5. Schlieren photographs of the homogeneous jet. (a) Schlieren—knife edge parallel to jet axis. (b) Schlieren—knife edge perpendicular to jet axis.

error in ρ will be about 0.8 mg/cm^3 . If the same error occurs near the edge of the jet, the error in ρ will be only $\frac{1}{10}$ as large. Usually, however, the $\delta(y)$ curve is horizontal at the jet center, so the smaller error in $\delta(y)$, 0.03, should apply, and the error in ρ will be proportionally smaller. Furthermore, the $\delta(y)$ curve is smoothed so that the error is spread over neighboring zones, enters into the sum, and tends to reduce itself.

Probably the major source of error arises from local fluctuations in the jet density, which disturb its cylindrical symmetry, and from random fluctuations in the density of the room air in the interferometer beams (see Section III, A for moving film records of the jet). A safe limit for the absolute error is 10 percent. Density values are probably self-consistent within 5 percent.

III. EXPERIMENTAL RESULTS

A. The Homogeneous Open Jet without Models

The edge of the orifice of the jet represents a region where the bounding medium changes from metal to air. A disturbance always arises at this point, and is propagated into the jet at the local Mach angle (36° to the axis for $M = 1.70$). It is desirable to limit the working section to the conical region bounded by the plane of the orifice and this conical Mach wavelet. If the jet emerges at less than atmospheric

pressure, it contracts, and a compression shock sets in from the lip at angles greater than the Mach angle, thus further restricting the working section. Higher pressures than atmospheric cause the jet to expand, the expansion region beginning at the Mach wavelet from the lip, but the size of the working section remains unchanged. Thus it is desirable to maintain the jet pressure at atmospheric or slightly higher. Equation (2) gives $P/P_0 = 0.203$ for $M = 1.7$; accordingly, the necessary tank over-pressure is 58 p.s.i. if P is to be one atmosphere (14.7 p.s.i.).

Shadow, schlieren, and interference photographs were taken of the jet over a range of pressures both higher and lower than this. The

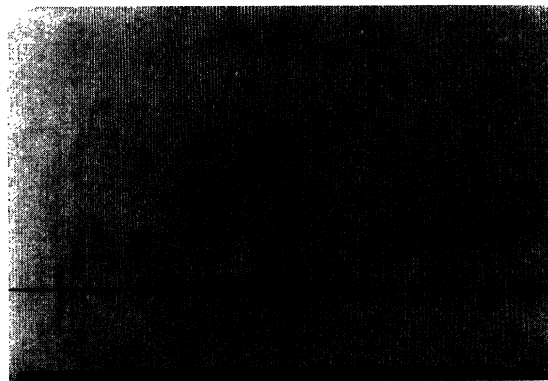


FIG. 6. Interferogram corresponding to the jet of Fig. 4.

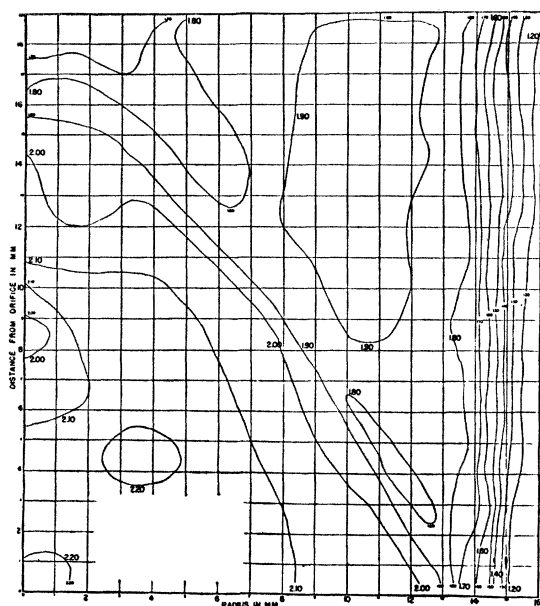


FIG. 7. Isopycnal chart for the homogeneous jet without model.

interferograms were each analyzed at three cross sections, located 1, 12, and 23 mm from the jet orifice. The general result showed that below 60-p.s.i. tank over-pressure a compression shock occurred, and that at 80 p.s.i. very definite expansion regions arose. Accordingly, a working over-pressure of about 69 p.s.i. was selected. This corresponds to an absolute pressure of 5.7 atmos., and at a temperature of 301°K to a density of 6.71 mg/cm³. Shadow, schlieren, and interference photographs of the jet at 69.5 p.s.i. are shown in Figs. 4, 5, and 6. Figure 7 gives a complete density analysis of the jet ("isopycnal chart"), and represents the averaged results of two photographic plates. The averaging was carried out on the fringe shift curves before the reduction process.

The density in the working section was 2.10 ± 0.1 mg/cm³, whereas the undisturbed air had a density of 1.20 at the prevailing pressure and temperature. Since the pressure in the working section was slightly higher than atmospheric, a weak conical expansion wave originated from the edge and reduced the density just outside this conical region from about 2.1 to 1.9 (see Fig. 7). Besides, the 2.2 isopycnic line (contour of density 2.2 mg/cm³) always appears near the center of the orifice. Various other "islands" in

the working section do not appear invariably and probably are due to accidental fluctuations.

If the viscosity and the heat conductivity of the gas are neglected, knowledge of the density and the initial conditions enables one to calculate the pressure P , temperature T , Mach number M , and flow velocity U in the jet. When the jet is free of shocks the adiabatic law may be used starting from the tank where U and $M=0$. As long as the density ratio in the shocks is <1.4 , as in the case in our homogeneous jet, the use of the adiabatic law does not introduce errors greater than 1 percent. Across stronger shocks, such as occur by inserting objects (see Section III, B, C, D), U , P , T , and M are connected by the Rankine-Hugoniot equations (Eqs. (9) in Section III, B). In the regions downstream from a shock, within a region free of rotational flow, the adiabatic laws may be used again, beginning with the conditions just after the shock. Once the temperature is known, the flow velocity may be calculated from the energy law which holds anywhere in the jet:

$$U^2 + 2C_p T = \text{constant} = 2C_p T_0,$$

where T_0 is the tank temperature and C_p the specific heat at constant pressure (1.00×10^7 erg/g°K). Table I gives pressure, temperature, Mach number, and velocity for each isopycnic line in the adiabatic undisturbed region of the homogeneous jet, together with the exact initial conditions and the equations used. However, this table is valid only inside the 1.80-mg/cm³ contour, because of mixing of the jet with the atmosphere outside this line. It is obvious that in this region of "mixing," viscosity, and heat conductivity cannot be neglected as was assumed at the beginning of this section. Also rotational flow may occur in a turbulent region.

As a check on the validity of the Mach numbers obtained from the density, Mach number values were measured directly with a multiple probe consisting of five 10° semi-angle cones. The head wave angles were measured from shadowgrams of the type shown in Fig. 8, and the Mach number was then obtained from the Taylor-Maccoll curves (see Section III, B). Actually the head wave angle differs but slightly from the Mach angle for this cone size and Mach number.

The Mach numbers obtained with the multiple

probe are considered to be the correct values; those obtained from the measured densities are correct only if the entropy has not changed in the flow of the gas from the pressure tank to the region under consideration. They agree with each other within about 1½ percent, but only in a region limited by the orifice as base and the conical expansion wave mentioned above. In this region the flow is nearly homogeneous within the experimental accuracy. The results show further that the jet is surrounded by a boundary layer in the form of a cylindrical sheath of approximately 4-mm width, where the actual Mach numbers obtained by the probe are appreciably less than the computed values due to the influence of friction and heat conductivity.⁹

In spite of the thick boundary layer, the Mach number calculated from the ratio of the area of the "throat" and the orifice (see Section II, A) agrees within one percent with the Mach numbers measured. This agreement is probably due to the fact that the boundary layer is already developed in the throat so that the ratio of the effective area of the streaming gas is not appreciably different from the ratio of the geometrical areas of the nozzle.

One further examination of the jet was made, namely, that of high speed moving film records. Vertical fringes formed by the intense constant light of a G.E. AH-6, 1-kw mercury arc operated on d.c. (with light filter for singling out the green line 5461A) were focused on a 0.2-mm aperture horizontal slit, placed just before the moving film of a General Radio Type 651-AE recording camera. The points, formed wherever a bright fringe crossed the slit, were drawn out into traces as the film moved, providing a time record of the sidewise motion of the fringes. The camera is adapted for standard 35-mm film and was run at the rate of about 1 cm per millisecond. A typical record is shown in Fig. 9 (cross section near orifice). On this picture the distance between successive perforations is about 500 microseconds. The section at the bottom shows the appearance of the undisplaced fringes before the opening of the valve. The cross section viewed by the slit is about 4 mm from the orifice. The magnification in this figure is about half that of Fig. 6.

⁹ For details see NAVORD Report 93-46.

TABLE I. Values of the gas dynamical variables (pressure, etc.) corresponding to density values in the homogeneous jet. (On the basis of the adiabatic law.) (Refers to Fig. 7.) $P/P_0 = (\rho/\rho_0)^\gamma$, $T/T_0 = (\rho/\rho_0)^{\gamma-1}$, $M^2 = U^2/a^2 = 2[T_0/T - 1](\gamma - 1)$, $U^2 = 2C_p(T_0 - T)$, $\gamma = C_p/C_v = 1.404$, $C_p = 1.00 \times 10^7$ erg/g °K, $\rho_0 = 6.708$ mg/cm³, $P_0 = 5.72$ atmos., $T_0 = 301^\circ K$.

Density ρ (mg/cm ³)	Pressure P (atmos.)	Temperature T (°K)	Mach number $M = U/a$	Velocity U (meter/sec.)
1.5	0.698	164	2.03	523
1.6	0.764	169	1.97	514
1.7	0.832	173	1.91	506
1.8	0.902	177	1.86	498
1.9	0.974	181	1.81	490
2.0	1.046	184	1.77	484
2.1	1.120	188	1.72	475
2.2	1.196	192	1.68	467
2.3	1.273	195	1.64	460
2.4	1.351	199	1.59	452
2.5	1.431	202	1.56	445

The principal feature of these records is the revelation of rapid changes in density that appear simultaneously across the entire jet and reoccur irregularly. These density fluctuations produce a fringe shift fluctuation of as much as two units.

A similar photograph made with the jet displaced just out of the interferometer light path showed that the main effect was in the jet itself, and that smaller additional effects were caused probably by the disturbance propagating away from the jet in the direction of the light path. The duration of these disturbances is too long for true turbulence, rather, they are to be associated with sound vibrations, plainly audible



FIG. 8. Direct measurement of Mach number with probes in the homogeneous jet. Probe semi-angle 10°. $M = 1.70$.

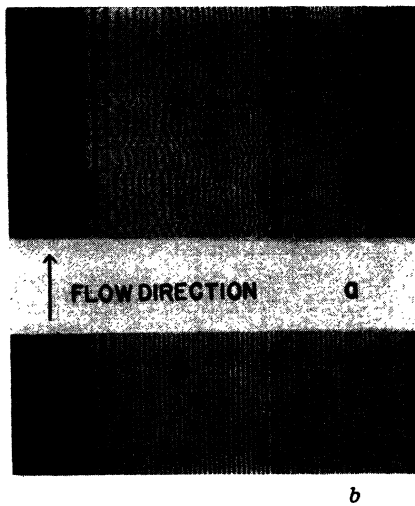


FIG. 9. Moving film records of the homogeneous jet at the cross section marked by the horizontal line in Fig. 6. (a) Jet on—displaced fringes. (b) Jet off—undisplaced fringes.

as the hissing of the discharge, perhaps due to fluctuations of the boundary layer in the nozzle.

Such disturbances are, of course, undesirable, and they explain the need for short exposure times, but their effect on the results of the measurements is probably not serious as the jet is quasi-stationary with respect to their duration time. The spark light source ($1-1\frac{1}{2}$ $\mu\text{sec.}$) used for interferometry, on the other hand, reveals true turbulence as small fluctuations which differ at various parts of the field. The slit aperture used for the moving film records corresponds to

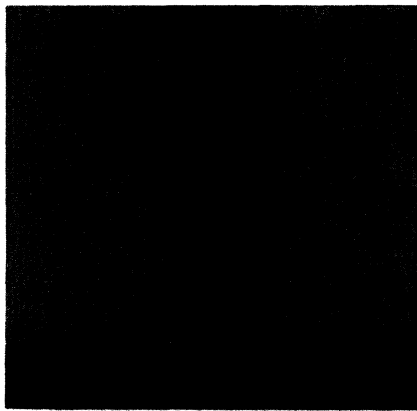


FIG. 10. Shadowgram of air flow about 30° semi-angle cone. Homogeneous jet, $M = 1.70$.

about 20 $\mu\text{sec.}$, so that true turbulence would not be resolved.

B. The Air Flow about a 30° Semi-Angle Cone in the Homogeneous Open Jet

Shadow, schlieren, and interference photographs were made of three cone sizes, chosen, respectively, to give a weak effect (10° semi-angle), a medium effect (30° semi-angle), and a strong effect with detached head wave (45° semi-angle). The results of Taylor and Maccoll,¹⁰ giving the theoretical flow about the 10° and 30° cones, were available for comparison with the measurements. To date no theoretical calculation has been made of the flow in the case of the detached head wave of a cone. The effect on the 10° semi-angle cone turned out to be so small the accuracy of the results obtained was rather poor. Inasmuch as the essential features are the same as for the 30° semi-angle cone, where the results have appreciably higher accuracy, only these are given here.¹¹

Shadow, schlieren, and interference photographs of this cone suspended in the homogeneous open jet are reproduced in Figs. 10–14. Figure 13 has been specially made to trace the course of a single fringe through the interferogram by using the complete spectrum of the spark and, accordingly, only the zero-order or “white light” fringes are visible. The isopycnal chart is given in Fig. 15. It is obtained from two separate interferograms, which were reduced and averaged. In this way accidental fluctuations are largely smoothed out. The chart was drawn from the analysis made at 6 cross sections of each interferogram, spaced every 2 mm between 0.5- and 10.5-mm distance from the orifice.

The general features of the homogeneous jet, shown in Fig. 7, are here exhibited upstream from the oblique conical shock head wave; namely, the general density of about 2 mg/cm^3 , a decrease through the boundary layer down to the atmospheric density of 1.2 mg/cm^3 , and the weak expansion region proceeding up from the

¹⁰ (a) G. I. Taylor and J. W. Maccoll, “The air pressure on a cone moving at high speeds,” *Proc. Roy. Soc.* **139**, 278, 298 (1933); (b) J. W. Maccoll, “The conical shock wave formed by a cone moving at high speeds,” *Proc. Roy. Soc.* **159**, 459 (1937).

¹¹ For the results obtained with the 10° cone see NAVORD Report 93–46.



FIG. 11. Schlieren photograph of air flow about a 30° semi-angle cone. (a) Knife edge normal to axis. (b) Knife edge parallel to axis.

corner of the jet. However, downstream from the strong shock wave the flow pattern is completely changed and shows the characteristic features of a flow about a cone, namely, the large compression of the air before the slant face of the cone starting at its tip, the large expansion around the shoulder, and the more or less conical regions arising from the tip and shoulder. The shock wave is accurately straight over most of its length, and the measured angle ($54.7^\circ \pm 0.2^\circ$) agrees well with the theoretical angle (54.66°) as given by Taylor and Maccoll for such a cone at a Mach number of 1.70. The shock angle and its strength decrease after the first expansion wavelet from the shoulder reaches out to the shock. There is also a small increase of strength and angle near the tip (see discussion below).

The values of pressure, temperature, Mach number, and velocity in the conical region between head wave and surface of the cone are listed as functions of the observed density in Table II, which has been derived on the assumption of adiabatic conditions after the shock wave. The equations used and the initial values are given in Table II also. The pressure, P_2 , and temperature, T_2 , on the downstream side of the head wave are obtained from the corresponding values on the upstream side by use of the Rankine-Hugoniot equations (see below).

The check between the theory of Taylor and Maccoll may be made by comparing—besides the head wave angle—the following factors:

1. The assumption that there is a conical region between the cone and its head wave, i.e.,

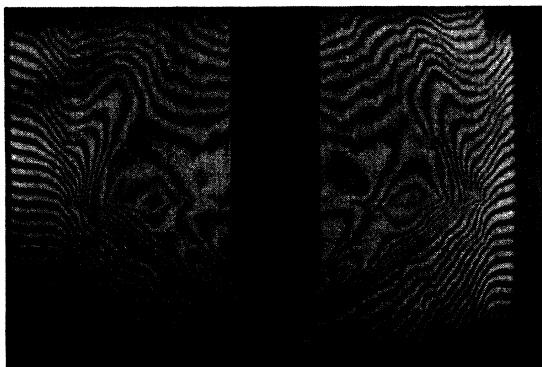


FIG. 12. Interferogram of air flow about 30° semi-angle cone. Fringes perpendicular to flow.

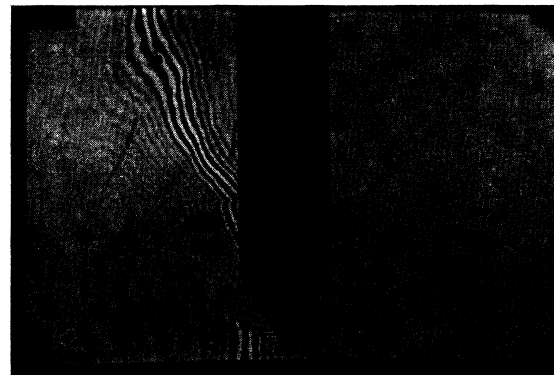


FIG. 13. Interferogram of air flow about 30° cone using "white light fringes."

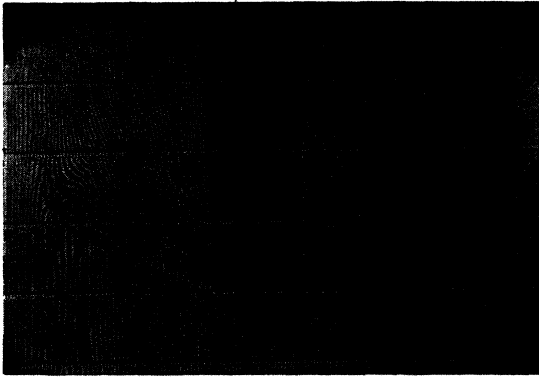


FIG. 14. Interferogram of air flow about 30° cone. Fringes parallel to jet.

that all variables are functions of θ only, where θ is the angle between the axis of the cone and a radius vector starting at the tip of the cone.

2. The actual value of the density ρ at the angle θ .

3. The pressure coefficients, $(P_s - P_1)/\rho_1 \bar{U}_1^2$, on the conical surface where index 1 refers to the conditions in the undisturbed homogeneous jet.

The check of the factors (1) and (2) is shown in Fig. 16. Here the density is given, for various angles θ , as a function of the distance R from the tip of the cone. The observed values are represented by the solid lines. The theoretical straight lines are dotted and are, of course, parallel to the R axis as the theory assumes this regime to be conical. The notation is the same as that used by Taylor and Maccoll. The theoretical values of the sound velocity, a , and the components of gas velocity along and normal to the radius vector, u and v , were furnished in tabular form for $\frac{1}{2}^\circ$ increments of θ for $M=1.70$, $\theta_s=30^\circ$, through the kindness of Dr. Z. Kopal of the Department of Electrical Engineering, M. I. T. From the initial reservoir conditions $P_0=5.72$ atmos., $\rho_0=6.71$ mg/cm³, and average observed Mach number in the working section, 1.705, the average pressure P_1 and density ρ_1 in the working section upstream from the shock regions were calculated by the relations

$$P_1 = P_0(1 + \frac{1}{2}(\gamma - 1)M^2)^{-\gamma/(\gamma - 1)}, \tag{7}$$

$$\rho_1 = \rho_0(1 + \frac{1}{2}(\gamma - 1)M^2)^{-1/(\gamma - 1)}, \tag{8}$$

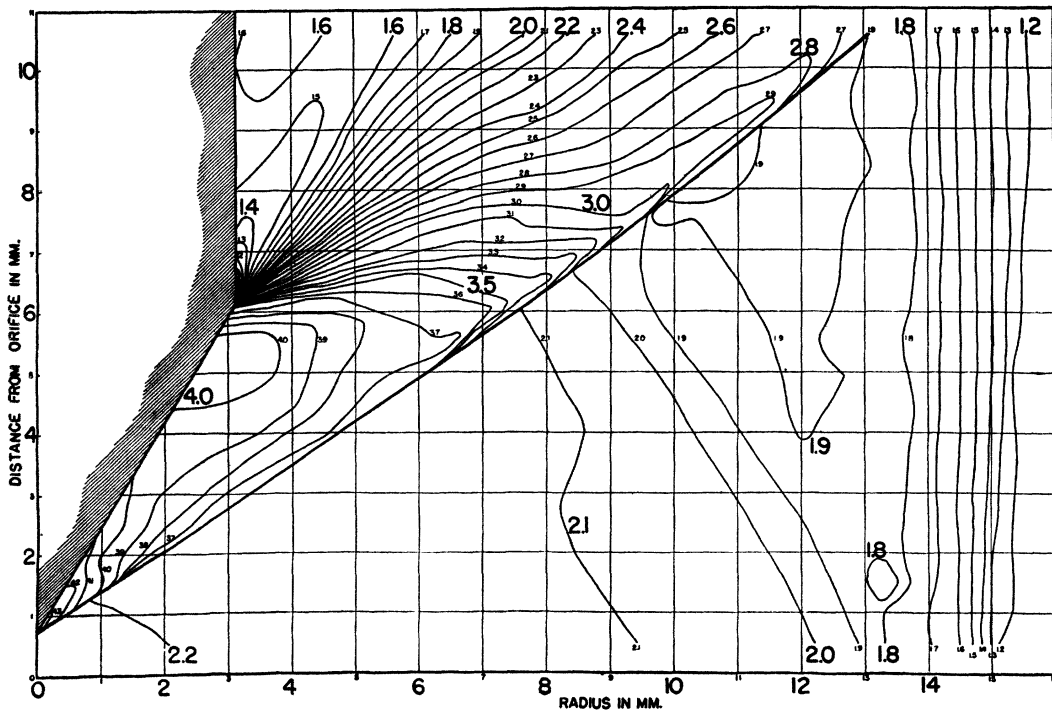


FIG. 15. Isopycnal chart for air flow about a cone of 30° half-angle. Mach No. 1.70. Contours labeled in mg/cm³.

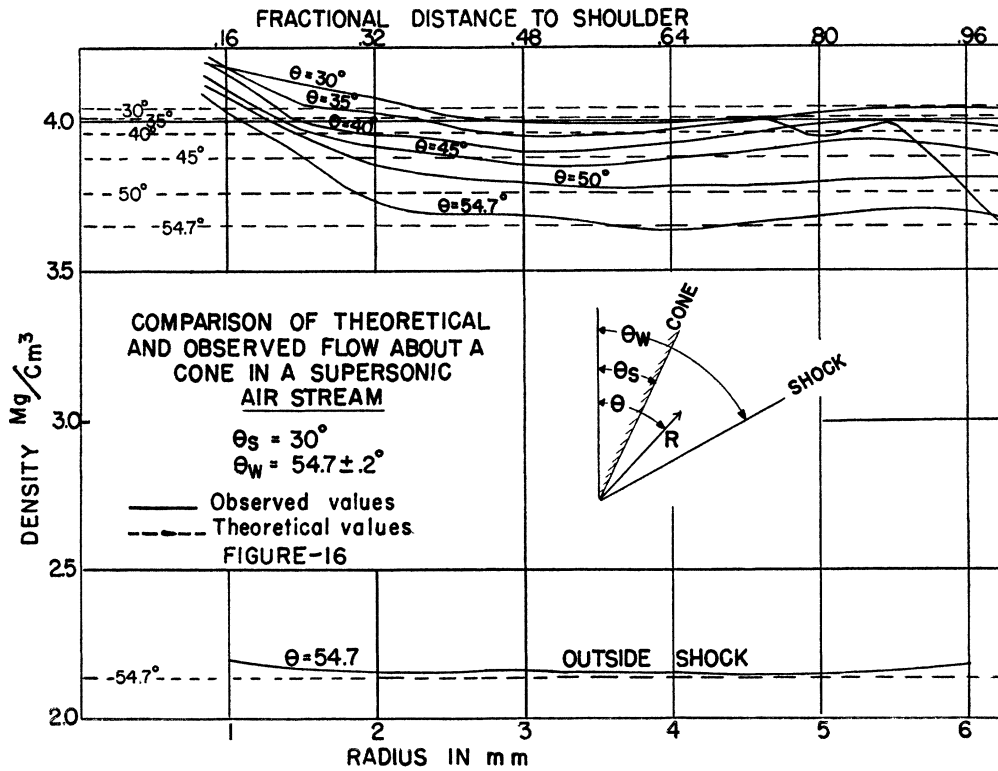


FIG. 16.

which assume isentropic flow through the nozzle (see also Table I). The pressure P_2 and density ρ_2 just after the shock were then calculated from the observed shock angle $\theta_w = 54.7^\circ$ and the Rankine-Hugoniot relations expressed in the form

$$\frac{P_2}{P_1} = \frac{[(\gamma+1)/(\gamma-1)](\rho_2/\rho_1) - 1}{[(\gamma+1)/(\gamma-1)] - \rho_2/\rho_1}$$

$$\frac{\rho_2}{\rho_1} = \frac{(\gamma+1)/2}{(1/M_n^2) + [(\gamma-1)/2]}$$

and

$$\frac{T_2}{T_1} = \frac{[(\gamma+1)/(\gamma-1)] - \rho_1/\rho_2}{[(\gamma+1)/(\gamma-1)] - (\rho_2/\rho_1)} \quad (9)$$

where $M_n = M \sin \theta_w$. The density in the region bounded by the cone and its head wave was then determined adiabatically, using the theoretical sound velocity at the desired values of θ with the aid of the relation

$$\rho = (\gamma c/a^2)^{1/(1-\gamma)}$$

which may be derived from the relations

$$P/\rho^\gamma = \text{constant} = P_2/\rho_2^\gamma = C, \quad \text{and} \quad a^2 = \gamma P/\rho.$$

In this calculation, the observable quantities

TABLE II. Pressure, etc., in the conical region for supersonic air flow about a 30° semi-angle cone at Mach No. 1.70. (Refers to Fig. 15.) $P/P_2 = (\rho/\rho_2)^\gamma$, $T/T_2 = (\rho/\rho_2)^{\gamma-1}$, $M = [2(T_0/T-1)/\gamma-1]^{1/2}$, $U^2 = 2C_p(T_0-T)$, $\gamma = 1.404$, $C_p = 1.00 \times 10^7$ erg/g $^\circ\text{K}$, $\rho_2 = 3.58 \times 10^{-3}$ g/cm 3 , $P_2 = 2.41$ atmos., $T_0 = 301^\circ\text{K}$, $T_2 = 237^\circ\text{K}$, $MT_2 = 1.15$.

Density ρ (mg/cm 3)	Pressure P (atmos.)	Temperature T ($^\circ\text{K}$)	Mach No. $M = U/a$	Velocity U (meter/sec.)
1.4	0.64	162	2.06	527
1.6	0.78	171	1.94	510
1.8	0.92	179	1.83	493
2.0	1.06	187	1.74	477
2.2	1.22	195	1.64	461
2.4	1.37	202	1.56	446
2.6	1.54	208	1.49	431
2.8	1.70	214	1.41	416
3.0	1.88	221	1.34	401
3.2	2.06	226	1.28	386
3.4	2.24	232	1.21	371
3.6	2.43	237	1.15	357
3.8	2.62	243	1.09	341
4.0	2.81	248	1.03	326
4.2	3.01	253	0.97	311
4.4	3.22	258	0.91	295
4.6	3.42	262	0.86	279

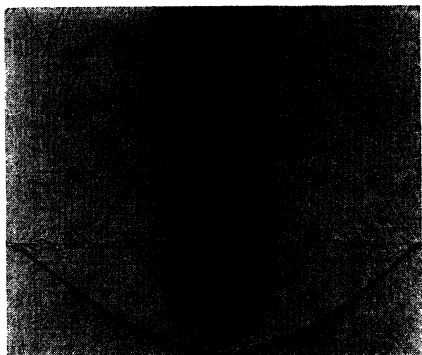


FIG. 17. Shadowgram of the air flow about a 45° semi-angle cone in a homogeneous jet. $M=1.70$.

which must be used to fix the theoretical values in the conical regions (shock angles, Mach number, and reservoir conditions) were chosen so as to involve the smallest experimental error without making use of the interferometer results. The air density values ρ in mg/cm^3 are plotted as ordinates in Fig. 16. Both the actual radial distance R in mm and the fractional distance between the cone point and shoulder are plotted as abscissae. The experimental results show slight variations of the density with R ; these may at least be partly due to variations of the density in the working section.

For $1 < R < 6$ mm the deviation from the conical regime outside the cone surface amounts to ± 7 percent maximum. For $2 < R < 6$ mm the deviation is only ± 1 percent maximum, with the absolute values of density in equally good agreement. On the surface ($\theta = 30^\circ$) the density drops rapidly near the shoulder. For $0.8 < R < 2$

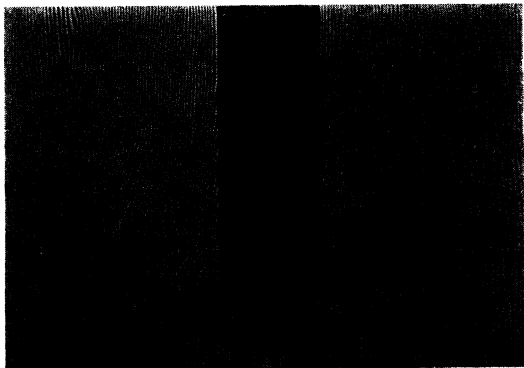


FIG. 18. Interferogram of the air flow about a 45° semi-angle cone in a homogeneous jet. $M=1.70$.

mm there is a systematic rise in density, as has also been found for the 10° cone. (One would expect that the shock angle at this point is also somewhat larger than at a greater distance from the tip of the cone, and this is actually observed (see Fig. 15)). It is reasonable to attribute this effect to the formation of a boundary layer on the cone surface, which is effective in making the cone slightly blunt; besides, the cone point was not ideally sharp. Further, the drop in pressure and density after the shoulder was propagated upstream along the surface in this boundary layer and produced the large drop in density for $\theta = 30^\circ$, $R > 4.5$ mm for $\theta = 54.7^\circ$, completely outside the headwave, the density is quite constant, and agrees closely with the average density for the working section, as shown by the dotted line at $\rho = 2.14 \text{ mg}/\text{cm}^3$ (Fig. 16). The pressure coefficient $K = (P_s - P_1)/\rho_1 U_1^2$ at the cone surface, calculated from the density $\rho_s = 3.98 \text{ mg}/\text{cm}^3$, with $P_1 = 1.164 \times 10^6 \text{ dynes}/\text{cm}^2$, $\rho_1 = 2.14 \times 10^{-3} \text{ g}/\text{cm}^3$, and $U_1 = 47100 \text{ cm}/\text{sec.}$, gives $K = 0.351$, whereas we would expect 0.352 from Taylor and Maccoll's results.

Taylor and Maccoll¹² give a comparison of the theoretical pressure coefficient with values measured in a wind tunnel with pressure holes on the conical surface. It is of interest that their values for hole "A" near the tip of the cone are higher, at least for the 20° and 30° cones, than theory would predict. This is in line with our observation of higher density near the tip. Besides this effect there is no systematic deviation of our results or of those of the wind tunnel experiments reported by Taylor and Maccoll from the theory.

In general, then, we may conclude that our results agree with Taylor and Maccoll's theory within the experimental error.

C. The Air Flow about a 45° Semi-Angle Cone in the Homogeneous Open Jet

(1) *Experimental Results*—Theory predicts that at Mach number 1.7 the head wave of this cone should be detached. This was found to be the case, as shown by the shadowgram of Fig. 17. The corresponding interferogram is given in Fig. 18 and the resultant isopycnal chart in Fig. 19.

One notices in the shadowgram of the 45° cone

¹² Reference 10(a), Fig. 12, p. 294.

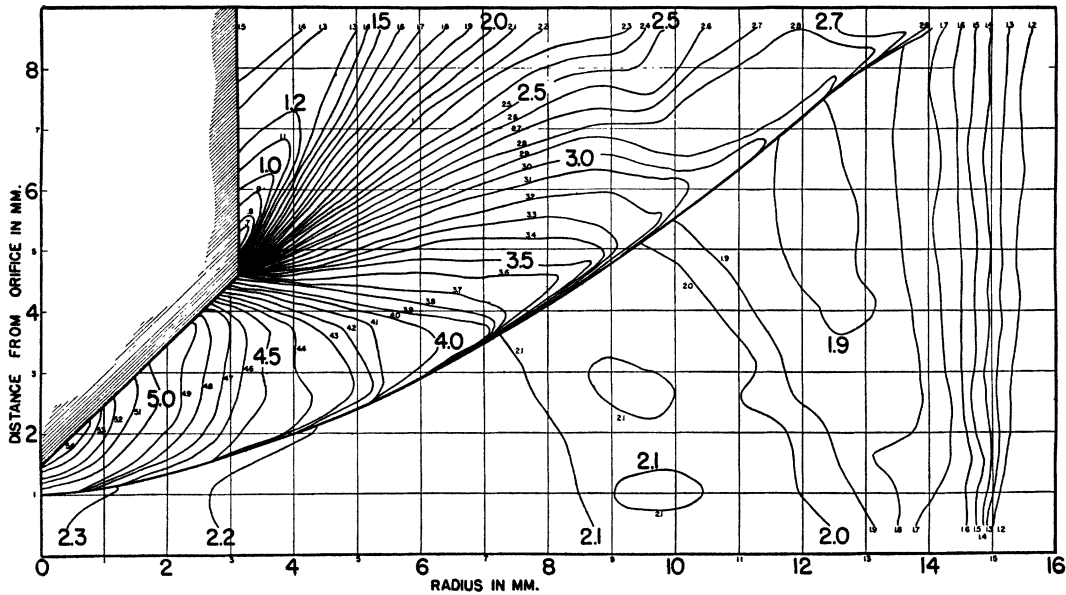


FIG. 19. Isopycnal chart for air flow about a cone of 45° half-angle. Mach. No. 1.70. Contours labeled in mg/cm³.

(Fig. 17) as well as in similar photographs of the 30° cone (Fig. 10) that appreciable distortion results from the strong refraction of the light. The cone shoulders, for example, appear to have projections which are actually not present. The schlieren photograph (Fig. 11) and, of course, the interferometric results (Figs. 15 and 19) reveal the region of very strong expansion at the shoulder which evidently causes the distortion in the shadowgram.

(2) *Calculation of Stream Lines*—In the case of the detached head wave, Taylor and Maccoll's theory breaks down as the regime around the cone is not of the simple conical type. The head wave is curved; consequently, the flow is rotational, and there is no simple way to calculate the pressure coefficient on the surface, or the values of pressure, temperature, and velocity at points in the flow field.

However, the interferometric results give the density at all points in the gas stream, and one is able to calculate the stream lines at each point in a stepwise approximate manner from well-established hydrodynamical relations. The simplest way is to use the equation of continuity, in the form $A \cdot \rho \cdot U = a$ constant, where A is the area between adjacent stream lines, corresponding to the density ρ and velocity U . The product

$A \cdot \rho \cdot U$ is fixed from known conditions upstream from the shock wave. The stream direction is everywhere parallel to the jet axis in this region. One computes the velocity U_2 on the downstream side of the shock from the usual Hugoniot equations, knowing U_1 on the upstream side and the shock wave angle θ at that point (see Fig. 20). If α is the deflection of the stream

$$U_1 \sin \theta = U_2 \sin(\theta + \alpha),$$

$$\frac{U_1 \cos \theta}{U_2 \cos(\theta + \alpha)} = \frac{1 + [(\gamma + 1)/(\gamma - 1)]P_2/P_1}{[(\gamma + 1)/(\gamma - 1)] + P_2/P_1},$$

$$P_2/P_1 = 2\gamma M_1^2 \cos^2 \theta / \gamma + 1 - [(\gamma - 1)/(\gamma + 1)].$$

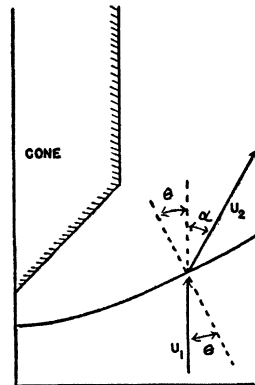


FIG. 20. Deflection of the gas stream in crossing an oblique head wave.

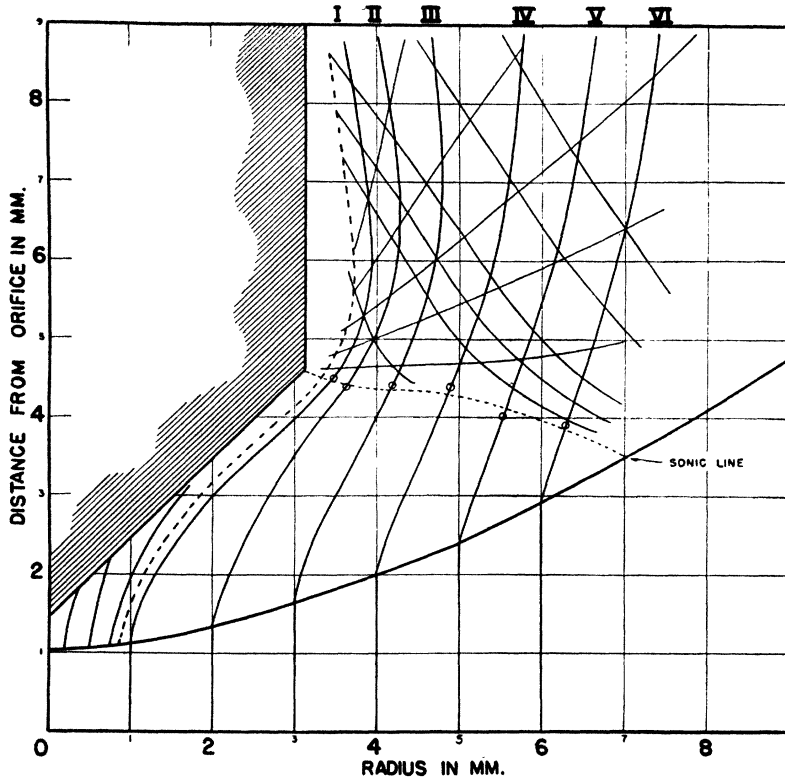


FIG. 21. Stream and Mach lines about a cone of 45° half-angle. Mach No. 1.70.

Therefore

$$U_2 = U_1 \sin \theta \left[\frac{1}{\tan^2 \theta} \left(\frac{1}{M_1^2 \cos^2 \theta} + \frac{\gamma - 1}{2} \right) + 1 \right]^{\frac{1}{2}}$$

$$\alpha = \left\{ \tan^{-1} \left[\frac{\frac{1}{2}(\gamma + 1) \tan \theta}{(1/M_1^2 \cos^2 \theta) + (\gamma - 1)/2} \right] \right\} - \theta.$$

TABLE III. Pressure coefficient on the surface of a 45° semi-angle cone. Mach number 1.70. (Refers to Figs. 19 and 21.)

$$K = \frac{P_s - P_1}{\rho_1 U_1^2} = \frac{0.361 \rho_s^{1.404} - 1}{408} \times 10^2$$

r—radius in mm, *z*—distance from orifice in mm

Location of point (<i>r, z</i>)mm	ρ_s mg/cm ³	K
(0, 1.5)	5.42	0.704
(0.52, 2.0)	5.44	0.709
(1.53, 3.0)	5.09	0.624
(2.53, 4.0)	4.74	0.541
(3.12, 4.57)	3.72	0.315
(3.12, 5.0)	0.70	-0.191
(3.12, 6.0)	1.00	-0.181
(3.12, 7.0)	1.25	-0.124
(3.12, 8.0)	1.43	-0.099

On the downstream side the values of *U* of each point are obtained from the measured ρ -values by use of the adiabatic relations and the gas law. Since $A \cdot \rho \cdot U$ is constant also, *A* may be calculated at each point in a stepwise approximate manner. Knowledge of *A* serves to fix the stream line position. In flows where the deflection of the stream is large, the approximations involved in this method become poor and the method is difficult to apply. Then another method, developed by one of the present authors (J. W.), may be used. It consists in a stepwise integration

TABLE IV. Pressure coefficient on the surface of a sphere at Mach number 1.70. (Refers to Figs. 24 and 25.)

$$K = \frac{P_s - P_1}{\rho_1 U_1^2} = \frac{0.359 \rho_s^{1.404} - 1}{408} \times 10^2$$

r—radius in mm, *z*—distance from orifice in mm

Location of point (<i>r, z</i>)mm	ρ_s mg/cm ³	K
(0, 4.)	6.1	0.869
(1.37, 4.20)	5.37	0.697
(2.66, 5.0)	3.87	0.344
(3.42, 6.0)	2.97	0.160
(3.80, 7.0)	1.90	-0.029
(3.88, 8.0)	1.20	-0.132

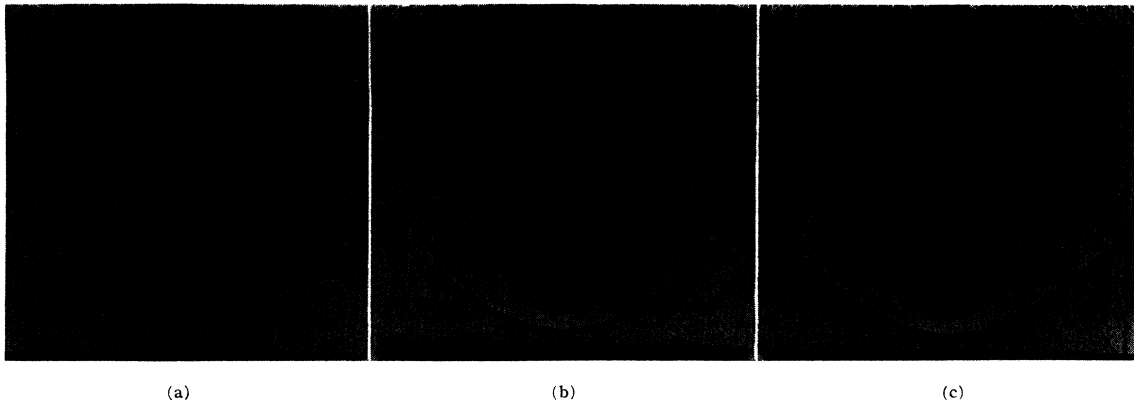


FIG. 22. Shadowgrams of air flow about a sphere in a homogeneous jet. $M=1.70$. (a) Plate—sphere distance = 25 mm. (b) Plate—sphere distance = 50 mm. (c) Plate—sphere distance = 100 mm.

of the equations of motion of the gas

$$dU/dt = -(\text{grad } P)/\rho,$$

considering that the measured isopycnals are identical with the isobars in a shock free region, except in cases of very large rotations,¹³ and that the stagnation temperature T_0 and pressure P_0 in the tank are known. Figure 21 shows typical stream lines constructed in this way for flow about the 45° semi-angle cone. This figure shows also the Mach lines. The Mach numbers and the local angle $\pm\phi$ between Mach lines and stream lines at any point may be calculated from the equation

$$M = U/a = 1/\sin\phi \\ = \pm \{2/(\gamma - 1)[(T_0/T_2)(\rho/\rho_2)^{1-\gamma} - 1]\}^{1/2}. \quad (10)$$

The sonic line may be located by setting $M=1$ in this equation and solving for ρ . The calculated points and the best line through them are also shown in Fig. 21 although it is evident that the sonic line does not simultaneously intersect the stream lines at $\phi=90^\circ$ and pass through the sonic points, as it should. This shows that the accuracy of the present results is not high.

Besides the velocity, temperature, and pressure along stream lines may be calculated adiabatically, starting after the shock wave. It turns out that the constants in these equations for the

different stream lines are the same within the accuracy of the experiments,¹⁴ showing that the rotational effects due to the curvature of the head wave may be neglected for these calculations. The equations for the pressure P in atmos., the temperature T in $^\circ\text{K}$, the Mach Number M , and the velocity U in meter/sec. are

$$P = 0.414\rho^{1.404}, \quad T = 144\rho^{0.404}, \\ M = 3.20(\rho^{-0.404} - 0.485)^{1/2}, \\ U = 533(2.063 - \rho^{0.404})^{1/2}(\text{meter/sec.}),$$

where ρ is in mg/cm^3 and $\gamma = C_p/C_v = 1.404$. For example, for 1 mm from the axis and 2 mm above the orifice one obtains for $\rho = 5.23 \text{ mg}/\text{cm}^3$, $P = 4.22$ atmos., $T = 282^\circ\text{K}$, $M = 0.526$, and $U = 179$ meter/sec.

The pressure coefficients K at several points on the surface of the 45° cone are given in Table III. They were calculated from the values obtained by inserting the surface density values ρ_s at the indicated places with coordinates (r, z) , as given in Fig. 19.

D. Examination of the Air Flow about a Sphere in the Homogeneous Open Jet

(1) *Experimental Results and Comparison of Shadowgraph Theory and Experiment*—Shadowgrams of the air flow about a sphere of $\frac{3}{32}$ -in. diameter, made with parallel light from a point

¹³ For details see NAVORD Report 93-46.

¹⁴ See NAVORD Report 93-46, Table III, p. 39.

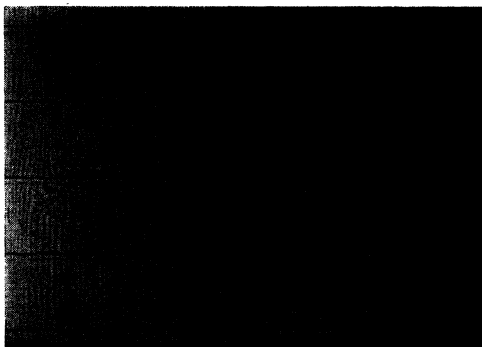


FIG. 23. Interferogram of the air flow about a 9/32-in. sphere in a homogeneous jet. $M=1.70$.

source, are shown in Fig. 22. The three photographs are all of the same phenomena but differ in appearance as the photographic plate was placed at different distances from the jet axis (25, 50, and 100 mm, respectively, for Fig. 22(a), (b), and (c)). The result is that the width of the dark band, representing the effect of the head wave, increases from (a) to (c). Other shadows change correspondingly, giving the appearance of over-all greater contrast. The theory of shadowgrams, as developed by Keenan and Polachek,¹⁵ enables one to determine the shock strength by measuring the width of the dark

bands on photographic plates placed at several known distances from the shock wave. For the shadowgrams of Fig. 22 these authors find $\rho_2/\rho_1=2.18$ for the shock strength on the axis as compared with $\rho_2/\rho_1=2.26$ measured by the interferometer. The shadowgraph method also gives the density gradient immediately after the shock; the spacing of the measured cross sections in our interferogram was not made small enough in this case to give a value of the gradient sufficiently accurate for comparison.

(2) *Interferometric Results*—The shadowgrams, as well as the interferogram of the same sphere (Fig. 23), reveal one drawback of the experimental arrangement; namely, that the head wave intersects the jet boundary on a level through the rear portion of the sphere. The disturbance caused by this intersection is in the path of the light beam all the way around the periphery of the circular jet and is severe enough to distort the fringes badly. Accordingly, Fig. 23 was measured only up to a horizontal line through the center of the sphere (the resulting isopycnal chart is given in Fig. 24). In the usual high speed wind tunnel with glass or metal walls, the length of working section is considered to be limited to the place where the reflected head wave intersects the axis. Here, however, the

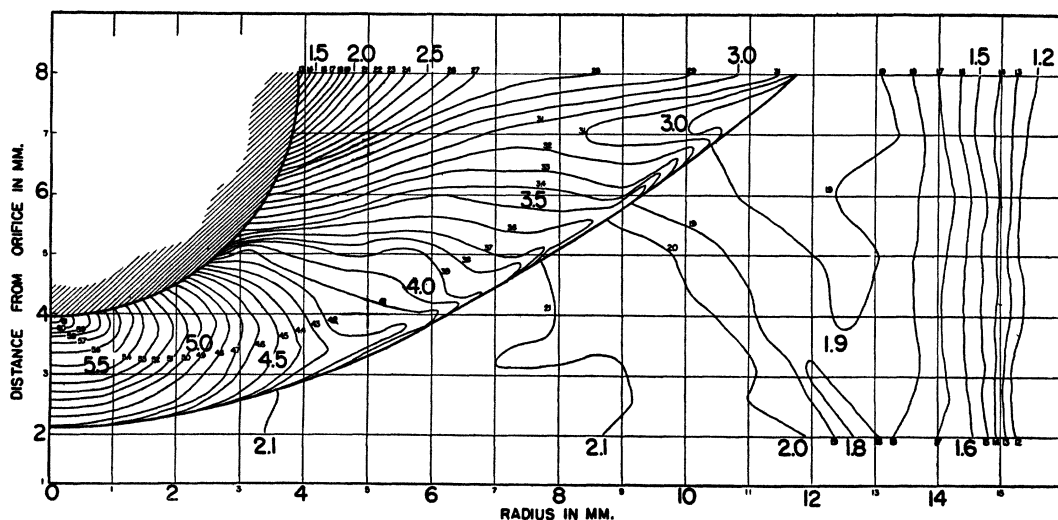


FIG. 24. Isopycnal chart for air flow about a sphere. Mach No. 1.70. Contours labeled in mg/cm^3 .

¹⁵ See P. C. Keenan and H. Polachek, "Measurement of densities in shock waves by the shadowgraph method," NAVORD Report 86-46.

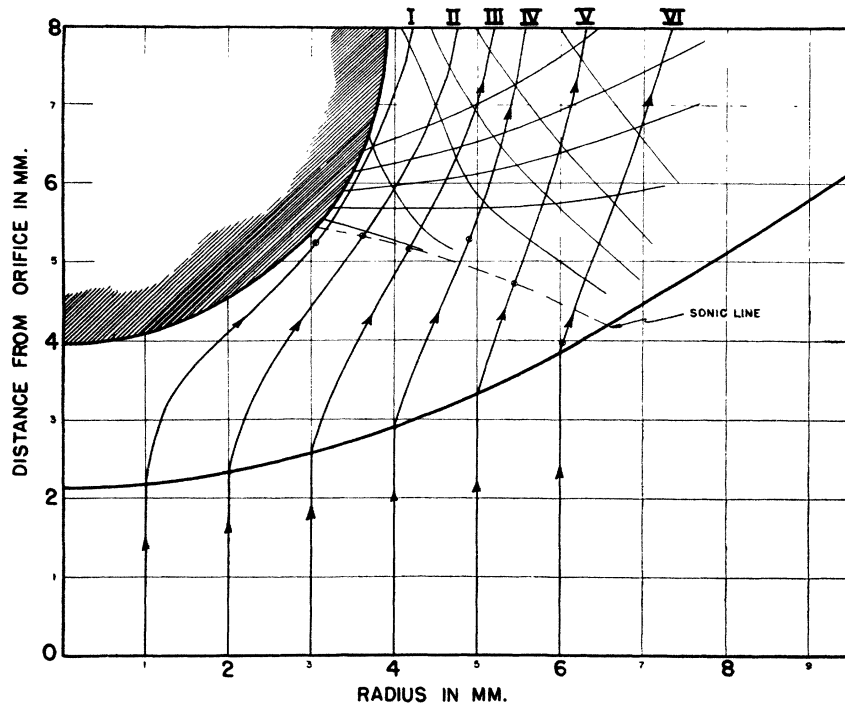


FIG. 25. Stream and Mach lines about a sphere. Mach No. 1.70.

working section cannot extend beyond the point where the head wave intersects the free boundary of the jet. Stream lines, Mach lines, and the sonic line have been calculated in the case of the sphere by the method outlined above for the 45° cone, and the results are given in Fig. 25. If pressure, temperature, Mach number, and velocity in the region between sphere and detached shock wave are calculated in the same way as for the 45° cone, the coefficients for the various stream lines show small differences, just outside the experimental accuracy, due to small rota-

tional effects.¹⁶ Pressure coefficients on the sphere surface are given in Table IV. They were calculated by use of the equation $P = 0.412\rho^{1.404}$ for stream line 1.

The results obtained indicate that for axially symmetric slender bodies, such as projectiles, surface pressures could be determined from the analysis of interferograms without exact knowledge of the stream lines, by making a reasonable guess at the path of the gas flowing along the surface.

¹⁶ See Table V in NAVORD Report 93-46.

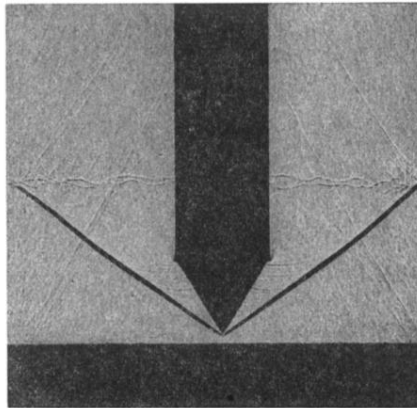


FIG. 10. Shadowgram of air flow about 30° semi-angle cone.
Homogeneous jet, $M = 1.70$.

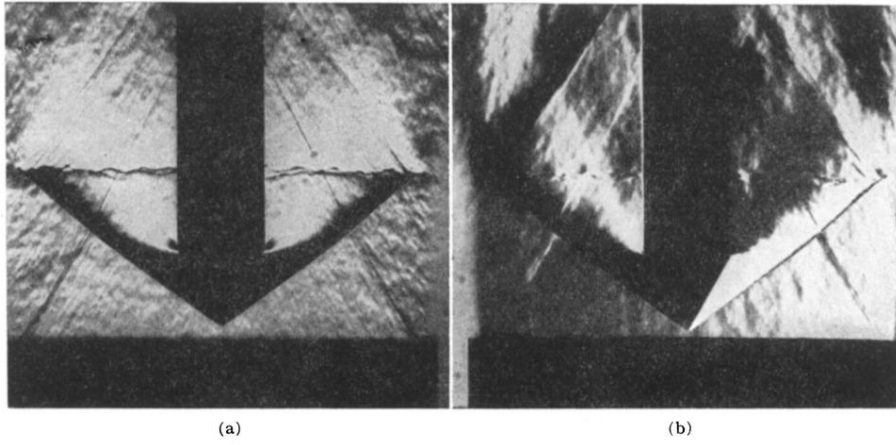


FIG. 11. Schlieren photograph of air flow about a 30° semi-angle cone. (a) Knife edge normal to axis. (b) Knife edge parallel to axis.

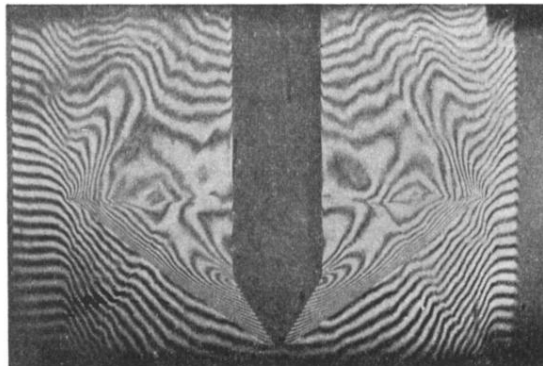


FIG. 12. Interferogram of air flow about 30° semi-angle cone.
Fringes perpendicular to flow.

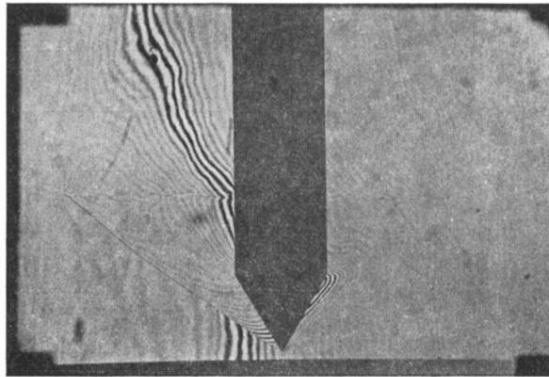


FIG. 13. Interferogram of air flow about 30° cone using
"white light fringes."

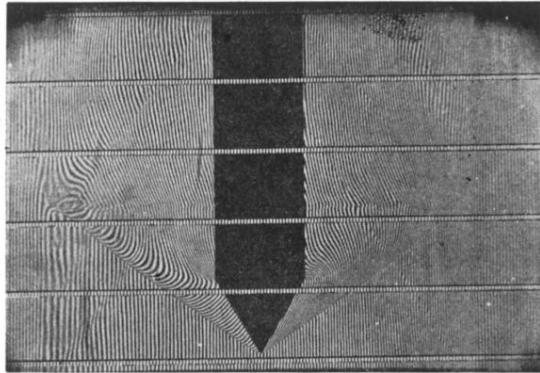


FIG. 14. Interferogram of air flow about 30° cone. Fringes parallel to jet.

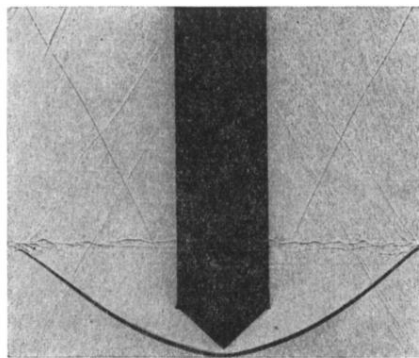


FIG. 17. Shadowgram of the air flow about a 45° semi-angle cone in a homogeneous jet. $M = 1.70$.

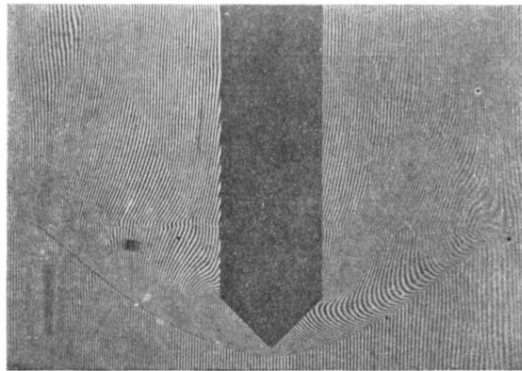


FIG. 18. Interferogram of the air flow about a 45° semi-angle cone in a homogeneous jet. $M = 1.70$.

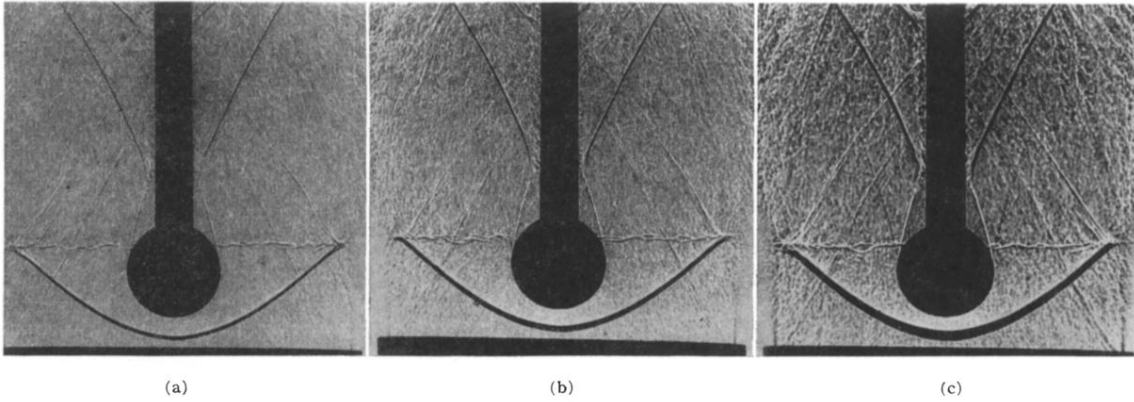


FIG. 22. Shadowgrams of air flow about a sphere in a homogeneous jet. $M = 1.70$. (a) Plate—sphere distance = 25 mm. (b) Plate—sphere distance = 50 mm. (c) Plate—sphere distance = 100 mm.

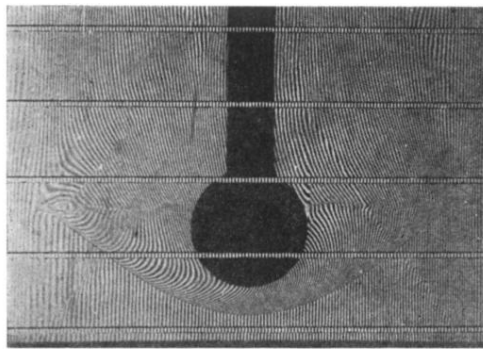


FIG. 23. Interferogram of the air flow about a $9/32$ -in. sphere in a homogeneous jet. $M=1.70$.

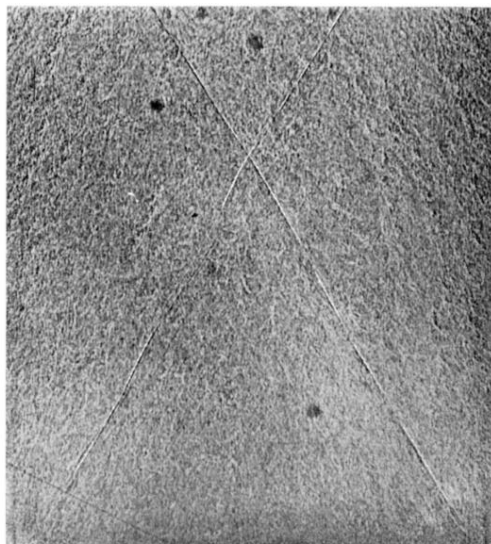


FIG. 4. Shadowgram of the homogeneous jet. $M = 1.70$.

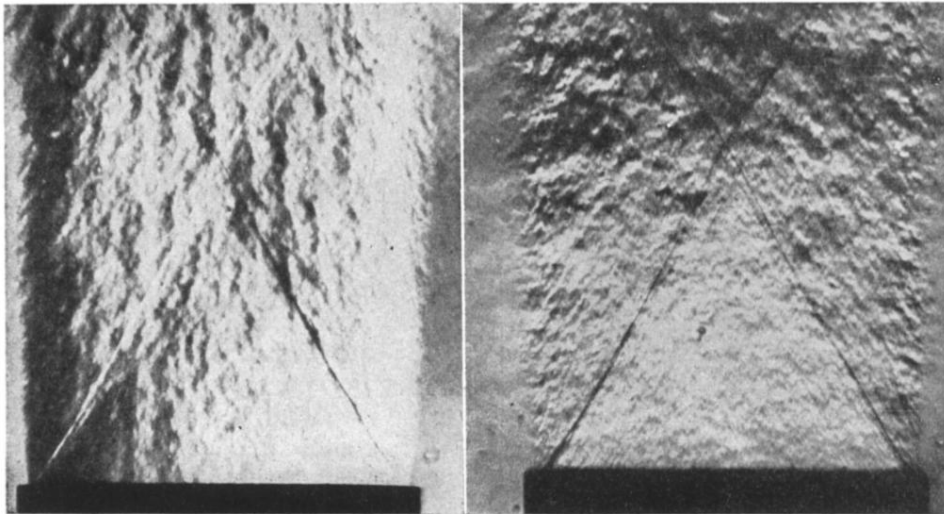


FIG. 5. Schlieren photographs of the homogeneous jet. (a) Schlieren—knife edge parallel to jet axis. (b) Schlieren—knife edge perpendicular to jet axis.

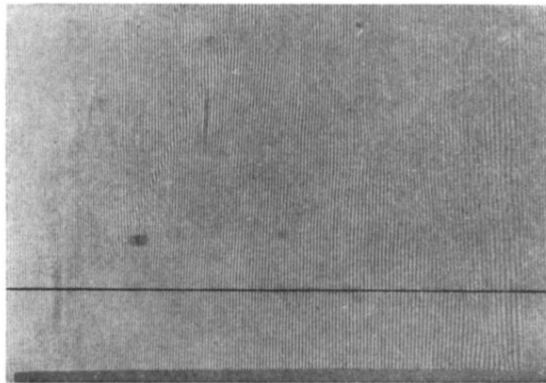


FIG. 6. Interferogram corresponding to the jet of Fig. 4.

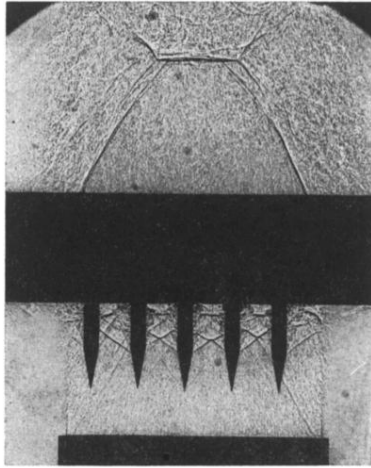
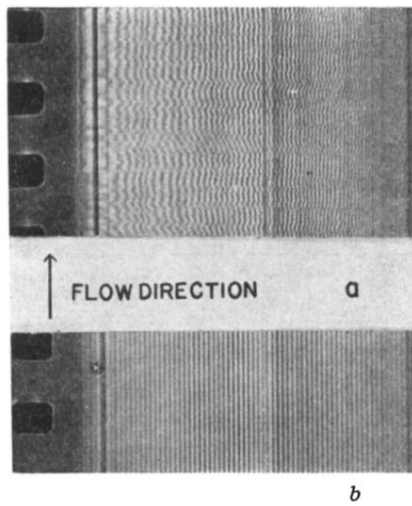


FIG. 8. Direct measurement of Mach number with probes in the homogeneous jet. Probe semi-angle 10° . $M=1.70$.



b

FIG. 9. Moving film records of the homogeneous jet at the cross section marked by the horizontal line in Fig. 6. (a) Jet on—displaced fringes. (b) Jet off—undisplaced fringes.